Applied Catalysis B: Environmental 198 (2016) 404–410

Contents lists available at ScienceDirect

Applied Catalysis B: Environmental

journal homepage: www.elsevier.com/locate/apcatb

# A nonanuclear nickel cluster-based coordination polymer for solar hydrogen production from water in open atmosphere

Ya-Nan Feng[a,b], Shao-Wu Du[a,*]

[a] State Key Laboratory of Structural Chemistry, Fujian Institute of Research on the Structure of Matter, Chinese Academy of Sciences, Fujian, Fuzhou 350002, PR China
[b] University of Chinese Academy of Sciences, Beijing 100039, PR China

ARTICLE INFO

*Article history:*
Received 21 April 2016
Received in revised form 26 May 2016
Accepted 28 May 2016
Available online 31 May 2016

*Keywords:*
Cluster-based CP
Solar-driven $H_2$ production
Aerotolerance

ABSTRACT

In this work, a novel 2D double-layered metal-organic coordination polymer, $[Ni_9(Hmna)_2(mna)_8(H_2O)_{10}]\cdot(H_2O)_{11}$ (**1**) ($H_2$mna = 2-mercaptonicotinic acid), based on a nonanuclear nickel cluster was synthesized to function as an efficient heterogeneous catalyst with an optimized TON of 685.4 for solar-driven $H_2$ production from water. Both the solar conversion and water utilization were achieved simultaneously in this photocatalytic system. Without the protection of inert atmosphere, the catalyst was still able to produce hydrogen with a TON of 93.5 in air. The influence of oxygen was studied by virtue of cyclic voltammograms (CVs) and UV–vis adsorption spectrum. The active radicals generated in the photocatalytical process were examined by *in-situ* electron paramagnetic resonance (EPR) experiments which provided solid evidence to support the reductive mechanism.



## 1. Introduction

The production of fuels from sunlight represents one of the major challenges to the development of a sustainable energy system [1–5]. Molecular hydrogen is the simplest fuel to produce which is considered to be an ideal "green" energy carrier and potential transportation fuel for the future. Platinum and other noble metals are efficient catalysts for photo-hydrogen evolution. However, for large scale use, it is urgent to explore new cost-effective materials with high efficiencies to replace these noble-metal catalysts.

Metal-organic coordination polymers (CPs) are a new class of hybrid inorganic-organic materials constructed by nodes of metal ions/clusters and multitopic organic linkers. Benefiting from their diverse structures and tailorable chemistry, CPs have become competitive candidates in some areas, such as chemical sensor, gas storage/separation and catalysis [6–15]. For solar hydrogen production, they have unique advantages as compared to other photocatalytic systems. Firstly, some of them, *e.g.* MIL-125, UiO-66 and their amino derivatives can act as semiconductors due to their appropriate valence and conduction bands that are suitable for use in photocatalytic $H_2$ evolving systems [16–20]. In addition, they can be designed as photosensitizers or catalysts by modifying the linkers or nodes with some specialized chromophores, such as Ru- and Ir-based complexes and phthalocyanine derivatives, or by incorporating photocatalytic active complexes like [FeFe]-hydrogenase mimics into the polymers [17,21–29].

Although photo-evolution of $H_2$ based on CPs has recently made some progress, the activity is still expected to be improved. In addition, the poor stability of CPs during the catalytic process greatly restricts their application in this area. Therefore, it is necessary and urgent to explore novel CP material with both excellent stability and high activity for photo-$H_2$ production.

The superior robustness of cluster-based CPs endows them with natural advantages in heterogeneous catalysis [30]. Some of the well-known cluster-based CPs and their derivatives, for example, have been successfully applied in the photocatalytic $H_2$ production systems that function in aqueous media owing to their high stability in water [16,18,19,24,25]. However, all these systems are operated under inert atmosphere and their ability to tolerate oxygen, which is a crucial issue to practical application, has not yet been explored. Herein, we report a 2D double-layered coordination polymer, namely $[Ni_9(Hmna)_2(mna)_8(H_2O)_{10}]\cdot(H_2O)_{11}$ (**1**) ($H_2$mna = 2-mercaptonicotinic acid), in which a nonanuclear Ni-S cluster serve not only as a connecting node of the polymer, but also as the photocatalytic center. With the help of the highly active

*Abbreviations:* CP, coordination polymer; CV, cyclic voltammetry; Fl, fluorescein; EPR, electron paramagnetic resonance; TEA, triethylamine; QE, quantum efficiency; TON, turnover number.

* Corresponding author.
*E-mail address:* swdu@fjirsm.ac.cn (S.-W. Du).

http://dx.doi.org/10.1016/j.apcatb.2016.05.072
0926-3373/

Ni-S site [31–35], compound **1** exhibits excellent performance in the photo-$H_2$ production with activity slightly higher than some noble-metal based CPs. Moreover, hydrogen was still able to be produced when **1** was suspended in the aqueous fluorescein (Fl) and triethylamine (TEA) just under the direct sunlight outdoors in open atmosphere, which is, as far as we know, firstly reported for the solar-driven system based on CPs.

## 2. Experimental

### 2.1. Materials and characterization

All chemicals were purchased and without further purification before use. The XML2 white light diode (LED) light was purchased from Cree Company and the light power was set to 2.02 W, which was measured by Yuanfang PMS-80_V1 system. The average light intensity of the white LED was measured to be 0.64 W/cm$^2$ by Yuanfang SPIC-200 spectral irradiance colorimeter. A Rigaku MiniFlex diffractometer was used to record the powder X-ray diffraction (PXRD) patterns of crushed single crystals in the 2θ range of 5–50°. The Bruker Vetex 70 was used to record the FT-IR spectrum and the Sartorius PB-10 pH meter was used to measure the pH value of the solution. The HRTEM diagrams were recorded on the field emission transmission electron microscope (FETEM) Tecnai F20 with the accelerating voltage of 200 kV.

### 2.2. Synthesis and characterization

A suspension of $NiCl_2{\cdot}6H_2O$, KOH and 2-mercaptonicotinic acid (1:2:1) in water (10 mL) was stirred in a Teflon pot before sealed in a stainless steel autoclave and heated at 453 K for one day. Pure yellow brown square crystals were obtained by filtration and repeatedly washed by water (yield 42% based on Ni). Anal. Found (%) for $[Ni_9(mna)_{10}(H_2O)_{10}]{\cdot}(H_2O)_{11}$: C 28.53 H 3.29 N 5.62 S 13.10. Calcd (%): C 29.01 H 3.06 N 5.74 S 13.14. FT-IR (KBr pellet, cm$^{-1}$): 3434.5 (s), 1586.7 (s), 1544.1 (m), 1443.8 (w), 1395.7 (s), 1263.0 (w), 1225.8 (w), 1151.4 (w), 1130.2 (w), 1093.1 (w), 1061.6 (w), 987.3 (w), 875.7 (m), 769.3 (m), 673.7 (w), 647.5 (w), 567.3 (w). UV–vis ($BaSO_4$, nm, Fig. S1): 306.6 (s), 363.7 (s), 675.0 (w).

Crystallographic data: $[Ni_9(Hmna)_2(mna)_8(H_2O)_{10}]{\cdot}(H_2O)_{11}$, $M_r$ = 2440.28, monoclinic, $P2(1)/c$, $a$ = 19.414(5) Å, $b$ = 22.268(5) Å, $c$ = 20.521(4) Å, α = 90°, β = 94.887(4)°, $\gamma$ = 90°, $V$ = 8840(3) Å$^3$, $Z$ = 4, $\theta_{max}$ = 27.49°, $\theta_{min}$ = 2.08°, $\rho_{calcd}$ = 1.834 g cm$^{-3}$, $\mu$ = 2.204 mm$^{-1}$, 20126 total reflections, 15869 observed ($I > 2\sigma(I)$), $R_1$ = 0.0617, $wR_2$ = 0.2430, GOF = 1.151. Other crystallographic data of **1** can be freely obtained from CCDC 1421257 in the Cambridge Crystallographic Data Centre.

### 2.3. Photocatalysis

Fluorescein and the ground catalyst **1** was added to an aqueous triethylamine (TEA) solution with the adjusted pH value in a Schlenk tube and the volume of the solution was kept at 10 mL. Before the illuminated by the white LED, the above mixture was freeze-pump-thaw treated for three times to keep the system under the specific atmosphere. If the photocatalytic test was conducted in the presence of air, no degassing treatment was carried out for the mixture before illumination. The hydrogen was monitored by gas chromatograph (Fuli 9790II) equipped with a thermal conductivity detector in negative polarity and a 5 Å molecular column (Φ3 mm × 3 m) heated at 353 K under argon atmosphere.

### 2.4. Quantum efficiency test

The Cree XTE sapphire blue LED (λ = 455 nm) and Cree XPE green LED (λ = 525 nm) were respectively used to replace the white LED in the quantum efficiency test in the presence of catalyst (5 mg), fluorescein (4 mM) and triethylamine (15%) with the pH value of 10. The average intensity of the light (I) was measured by Yuanfang SPIC-200 spectral irradiance colorimeter and the irradiation area (A) was 3.14 cm$^2$. The amount of produced hydrogen ($n_{H2}$) after the illumination for **1** h was determined by the GC and recorded in Table S1. The number of passed photons (F) was calculated based on the Eq. (1) and the quantum efficiency was calculated according to the Eq. (2).

$$F = \frac{E\lambda}{hc} = \frac{IAt\lambda}{hc} \quad (1)$$

$$QE = \frac{2n_{H2}N}{F} \quad (2)$$

In the Eq. (1), $t$ is the irradiation time, $h$ is the Planck constant, and $c$ is the speed of light. In the Eq. (2), $N$ is the Avogadro constant.

### 2.5. Isotope experiments

An identical amount of deuterium oxide and aqueous deuterium chloride were used to replace water and hydrochloric acid in typical photocatalytic experiments. After illumination for 48 h, 5 mL gas above the solution was syringed out and injected into the gas chromatograph (Fuli 9790II) equipped with a thermal conductivity detector in positive polarity and a TDX-01 molecular column (Φ3 mm × 2 m) heated at 353 K under helium. The identical amount of gas produced during the photocatalytic reaction was also used for mass spectrometry (MS) analysis on Hiden-qic-20 mass spectrometer.

### 2.6. Electrochemistry

Electrochemical experiments were carried out on a CHI 600D electrochemical potentiostat. Cyclic voltammograms were recorded in a three-electrode cell under specific atmosphere with a glassy carbon disc (diameter 3 mm) as working electrode, a Ag|AgCl electrode as reference electrode and a platinum wire as auxiliary electrode. A 0.1 M sodium perchlorate solution was used as electrolyte. Compound **1** (5 mg) was dispersed in a mixture of water (1 mL) and Nafion (5%, 50 μL) before ultrasonicated for 30 min. Afterwards, 5 μL of the resultant mixture was applied to the surface of glassy carbon. After drying under illumination of infrared lamp, Nafion (0.05%, 10 μL) in ethanol was coated on the surface of the catalyst and dried again before the electrochemical test.

### 2.7. UV–vis spectrum

Liquid samples (0.02 mL) were syringed out during the photolysis at different time and then diluted by 100 times with the same aqueous TEA solution to record the UV–vis spectrum on Perkinelmer Lamda35 UV/vis spectrometer. For solid state UV–vis spectrum of **1**, the solid sample was mixed with $BaSO_4$ and grinded prior to the measurement.

### 2.8. Fluorescence quenching experiments

The emission spectra of Fl (0.01 mM) was detected by R928 photomultiplier detector on a Cary Eclipse fluorescence spectrometer with the excitation wavelength of 460 nm from a flash xenon lamp when increasing amount of **1** and TEA were added as quenchers, respectively.

### 2.9. Zeta potential measurement

The catalyst (5 mg) was suspended in aqueous sodium hydroxide (10 mL) containing fluorescein (4 mM) at pH = 10 and sonicated

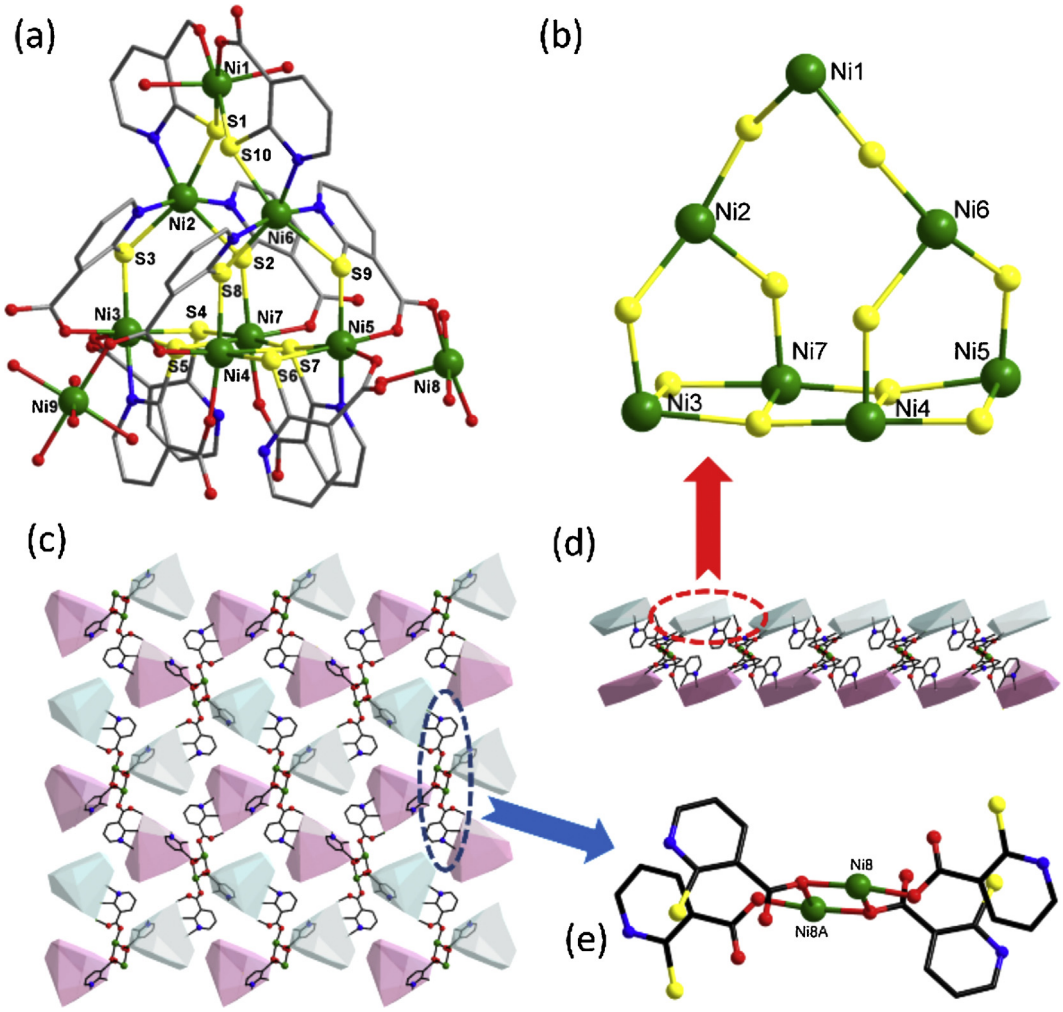


**Fig. 1.** (a) The structure of the nonanuclear nickel cluster. (b) The structure of $\{Ni_7S_{10}\}$ core. (c) View of the 2D layer along the a-axis. (d) View of the 2D layer along the *b*-axis showing the double-layered structure. (e) View of the dinuclear connecting node.

for 15 min before the 2 mL of the mixture was added to the quarts cuvette and test the zeta potential on Brookhaven BI-200SM laser particle size and zeta potential analyser.

### 2.10. In-situ *EPR*

All solutions were degassed by three freeze-pump-thaw cycles before equal volume of samples (20 μL) were syringed into quarts tubes and sealed with plasticine before the EPR test. All data was collected on Bruker-Biospin electron-paramagnetic resonance setting with unified parameters.

## 3. Results and discussion

### 3.1. Synthesis and structure

Yellow-brown microscopic crystals of **1** were prepared by the hydrothermal reaction of $NiCl_2$, $H_2$mna and NaOH (1:1:2) in 10 mL of $H_2O$ at 180 °C for one day. Compound **1** exhibits excellent stability towards air and water. The XRD pattern of the sample remains almost unchanged after being stored in air or soaked in water for several months (Fig. S2). The enhanced stability of **1** can be associated with the bridging and polychelating nature of the $H_2$mna ligand that is able to connect multi metal centers into a stable CP. Single crystal X-ray diffraction study reveals that **1** crystallizes in the *P*21/c space group and features a 2D double-layered cluster-based CP. The structure is composed of an unprecedented nonanuclear nickel cluster, which serves as a secondary building unit. This cluster contains nine crystallographically independent Ni(II) ions, eight $mna^{2-}$, two $Hmna^-$ and ten coordinated water molecules (Fig. 1a). All the Ni(II) ions are six-coordinated by S, N and O atoms from ligands and water molecules in a distorted octahedral coordination geometry. The presence of multiple donor sites in $H_2$mna ligand offers the possibility of coordination to more than one metal ions to generate a high-nuclear cluster. In **1**, the $Hmna^-$ anions adopt a $\mu_2$-$\kappa^2$S, $\kappa^1$O bridging mode with the protonated pyridine nitrogen atoms uncoordinated, while the $mna^{2-}$ dianions assume $\mu_2$-$\kappa^2$S, $\kappa^1$N, $\kappa^1$O, $\mu_3$-$\kappa^2$S, $\kappa^1$N, $\kappa^2$O,O' and an unusual $\mu_3$-$\kappa^3$S, $\kappa^1$N, $\kappa^1$O coordination mode, respectively. The most striking structural feature of **1** is the presence of a wax-jambo-shaped $\{Ni_7S_{10}\}$ cluster built upon seven Ni(II) atoms (Ni1, Ni2, Ni3, Ni4, Ni5, Ni6 and Ni7) and eight $\mu_2$-S and two $\mu_3$-S atoms (Fig. 1b). The Ni9 atom is anchored to the $\{Ni_7S_{10}\}$ cluster by the bridging carboxylate group while Ni8 and its symmetry-related atom form a dinuclear unit (Fig. 1d), which acts as a connecting node to organize the $\{Ni_7S_{10}\}$ clusters into a double layered CP (Fig. 1c).

### 3.2. Photocatalytical properties

Under inert atmosphere, the photocatalytic activity of **1** for $H_2$ evolution was investigated in an aqueous solution containing the

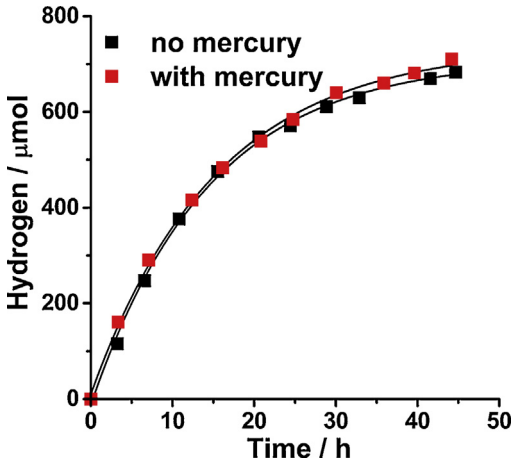


**Fig. 2.** The amount of $H_2$ generated in the absence or presence of mercury under the illumination of visible light.

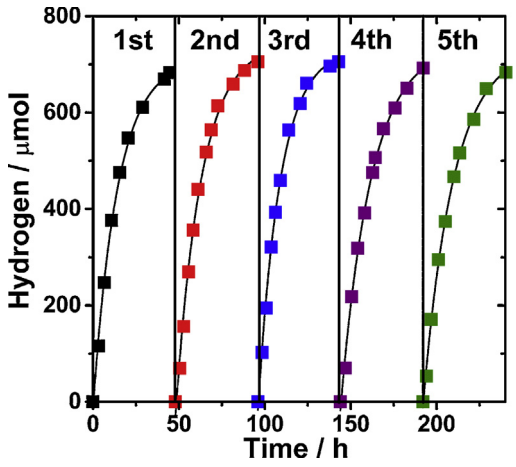


**Fig. 4.** Recycling test of **1** (10 mg) in argon atmosphere.

sacrificial electron donor TEA and the photosensitizer Fl. Every component among catalyst, photosensitizer, electron donor and illumination is indispensable in the photocatalytic tests. With the increasing pH and the ratio of TEA to water as well as the concentration of Fl, some positive effects were observed for both the $H_2$ evolution and the turnover number (TON, based on the catalyst, Fig. S3–5). By comparison, the influence of the dosage of catalyst on the $H_2$ evolution was a little complicated. Incremental $H_2$ was detected when the dosage of catalyst was increased from 1 to 5 mg. Further increase in the dosage of catalyst causes little increase in $H_2$ evolution (Fig. S6), which may be attributed to the change of rate-determining step from the amount of catalytic centers to the electron-transfer kinetics [36]. Meanwhile, the TON based on the catalyst was on the decline during the whole process for increasing the dosage of catalyst. The optimal TON of 685.4 in 48 h could be achieved when 1 mg of **1** was used with 15% (v/v) TEA and Fl (4 mM) at pH = 10. The quantum efficiency (QE) was calculated as 1.17% at 455 nm (Table S1). Such high efficiency is rare for the CPs-based photocatalytic $H_2$ production systems. To verify the heterogeneous nature of the catalyst, a series of control experiments were carried out. Under the same experimental conditions, much less $H_2$ was detected from the aqueous TEA and Fl solutions with equivalent amount of (i) $NiCl_2$, (ii) $H_2$mna, (iii) mixed $NiCl_2$ and $H_2$mna, or from the filtrate after stirring **1** with TEA and Fl in water (Table S2, Fig. S7). Furthermore, the addition of a small amount of mercury (0.5 mL) to the system did not significantly affect the photocatalytic activity, implying that the degradation of catalyst to metal nanoparticles did not occur during the photocatalytic process (Fig. 2) as the mercury might be apt to capture the potential metal nanoparticles to form amalgam and thereby decreasing the activity.[24]

After photocatalytic reaction for 48 h, the recovered catalyst still remained perfect crystallinity as shown from the clear lattice fringes in the high resolution transmission electron microscopy (HRTEM) images (Figs. 3 , S8), and no change was observed in both the IR and XRD analysis (Fig. S9), which indicated that the catalyst kept stable during the reaction. When the recovered catalyst was added to a fresh solution of TEA and Fl and under illumination again, $H_2$ was regenerated with the similar rate as before. Under the same conditions, the catalyst (10 mg) can be used repeatedly for five catalytic cycles without obvious loss of activity, and a total of 3474 μmol $H_2$ was generated (Fig. 4, Table S3). The catalyst can keep the high efficiency in 240 h, which is the longest lifetime among the CP-based systems for photo-$H_2$ generation. All these facts confirmed that **1** was the actual active center in this photocatalytic system.

### 3.3. Proton precursor

One of the primary goals of water-photolysis systems is to utilize the abundant source of water to produce clean fuel. In order to determine the proton precursor in our $H_2$ evolution system, isotope labelling experiment was conducted. The $H_2$ and $D_2$ gases evolved were distinguished by GC-TCD with TDX-01 column and helium as carrier. When the reaction was performed in $D_2O$, a positive peak corresponding to $D_2$ appeared at 0.47 min in the chromatogram,

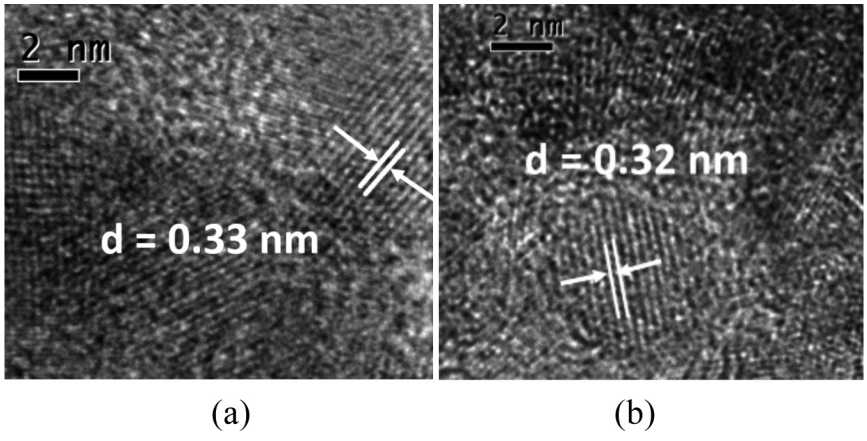


**Fig. 3.** HRTEM images of the fresh sample **1** (a) and the recovered sample **1** (b) after photocatalytic reaction for 48 h.

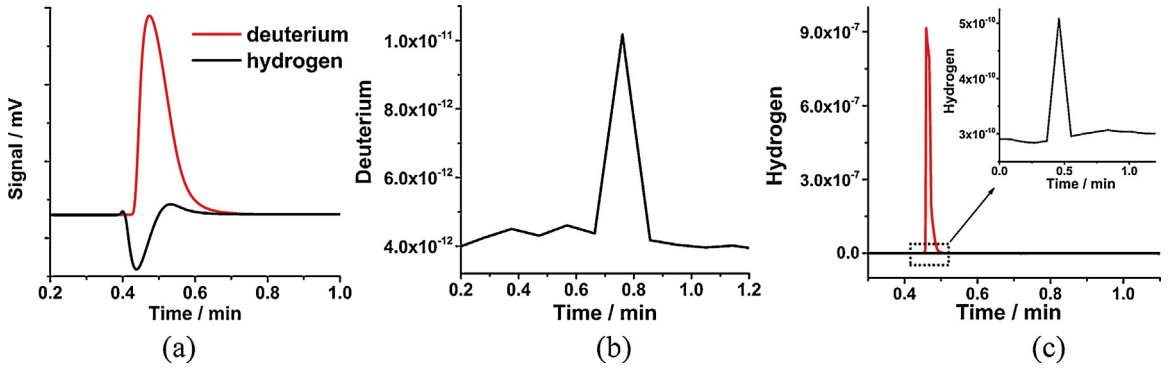


**Fig. 5.** (a) The signal response from the gas above the liquid when water and deuterium oxide were respectively used. (b) MS tracking signal of $D_2$ using $D_2O$ as solvent. (c) MS tracking signal of $H_2$ using $H_2O$ (red line) and $D_2O$ (black line) as solvent, respectively. Insert: the $H_2$ signal with $D_2O$ as the solvent. (For interpretation of the references to colour in this figure legend, the reader is referred to the web version of this article.)

which is different from the negative peak of $H_2$ at the close position (0.44 min) when water was used as solvent (Fig. 5a) [37]. This result indicates that our system is capable of catalysing water for making $H_2$. Further evidence that in this system $H_2$ was generated from water rather than other components comes from the MS analysis of the gases evolved. A signal corresponding to $D_2$ was detected from the photocatalytic reaction where $H_2O$ and HCl (for adjusting pH) were both replaced by $D_2O$ and DCl (Fig. 5b). Additionally, a very faint signal attributed to $H_2$ was also observed, which can be neglected because its peak height is three orders of magnitude lower than that obtained from the reaction in water (Fig. 5c). The trace amount of $H_2$ was possibly produced by the tiny hydrogen impurity in the isotopic reagent (99.8% purity).

### 3.4. Aerotolerant properties

Another goal of water-photolysis is to convert solar energy to chemical energy. When a capped test-tube consisting of the mixture was placed under direct sunlight on a sunny winter day in Fuzhou, China, sustained hydrogen production was observed, showing the capability for achieving sunlight conversion without precious metals (Fig. 6a,b). It is worth noting that in above experiment, the reaction was performed under aerobic conditions. When the reaction was conducted in an open atmosphere, a weak but still clearable signal for $H_2$ was detected from the gas above the liquid (Fig. 6c,d). These results indicate that our hydrogen evolving system can not only tolerate oxygen to a high extent (21% $O_2$), but also endure continued exposure to oxygen. Remarkably, the solar- driven $H_2$ evolution from water half-splitting in an open environment based on CPs has never been attempted before.

In order to study the influence of $O_2$ on the catalyst, we performed the photocatalytic experiment in a sealed Schlenk tube under different levels of $O_2$. With the increasing dosage of $O_2$, the amount of $H_2$ evolved was decreased (Fig. 7a). Nevertheless, more than 60% of the initial photocatalytic activity was retained under air atmosphere (Table S4) and the TON could reach up to 93.5 in 24 h when the reaction ceased. Furthermore, little irreversible damage of the catalyst was observed because it could be reused without appreciable loss of its activity after the addition of fresh fluorescein and TEA (Fig. S10). When the system was exposed to open atmosphere under the illumination of LED, diminishing signals for $H_2$ was detected by GC at one-hour intervals from the gas above the liquid (Fig. 7b), and the reaction finally ceased after 4.5 h. In spite of this, $H_2$ was able to be regenerated when the recoverd catalyst was added to the fresh aqueous Fl and TEA solution. And after five cycles, little shortening lifetime was observed, which demonstrated that the catalyst could resist the continuing exposure to $O_2$ in open atmosphere for a long period while producing $H_2$. The high oxygen resistance of **1** was also reflected in the CV experiment. Under argon atmosphere, the CV of **1** displayed a strong irreversible reductive wave around −1.03 V (*vs* Ag/AgCl), which was attributed to the electrocatalytic hydrogen evolution (Fig. 7c) [38]. Little difference on the onset potential and current was observed for the hydrogen evolution peak when the inert atmosphere was replaced by air. This indicates that the hydrogen production process is little inhibited by oxygen in a short time scale. Such $O_2$-tolerance in CV is firstly reported for Cps, and is rarely observed for $H_2$-evolving photocatalysts [39,40]. The superior aerotolerance may be originated from the high nuclearity of nickel cluster SBUs in **1** that can greatly improve the stability of both the CP and the intermediate oxidation state of the nickel ion [41].

In our system, the fast decomposition of Fl may be one of the reasons responsible for the negative influence of $O_2$. To test this hypothesis, liquid samples collected from the solution at different time during the photocatalytic reaction were analysed by UV–vis spectrum after dilution. It was found that the maximum adsorption of Fl at 496 nm was acceleratedly bleached with the increasing amount of $O_2$ under visible-light irradiation (Fig. S11). However, when fresh Fl was added to the residual solution at the end of the catalytic reaction, only a small amount of $H_2$ was regenerated under illumination in air (Fig. S12). This observation implies that like Fl, TEA is also $O_2$-sensitive under illumination, which might be supported by the fact that TEA can be excessively consumed by $O_2$ through photo-oxygenation [42]. In open atmosphere, except for light-induced damage of Fl and TEA by oxygen, the evident decrease in pH value of the solution during the reaction due to the sustained dissolution of carbon dioxide from air cannot be neglected. As a result, the reduction in lower pH levels can cause a lower concentration of both effective electron donors and photosensitizers, leading to a shortening of the lifetime of catalytic system. Indeed, when sodium hydroxide solution (pH = 12, 100 μL) was added to the residual solution after the photoreaction ceased, $H_2$ was regenerated for another half an hour. These experiments thus demonstrate that the excessive use of Fl and TEA can afford some protection against oxygen inactivation, which together with the superior stability of the catalyst enable the photo-$H_2$ evolution system to be operated under high levels of $O_2$, even in open atmosphere.

### 3.5. Photocatalytical mechanism

Steady fluorescein quenching experiments were conducted to study the photo-induced electron transfer (PET) process. The intensities of fluorescein gradually decreased with increasing TEA or **1**. In both cases the quenching effect followed the Stern-Völmer equation. The quenching constant was calculated to be 15 $M^{-1}$ for TEA

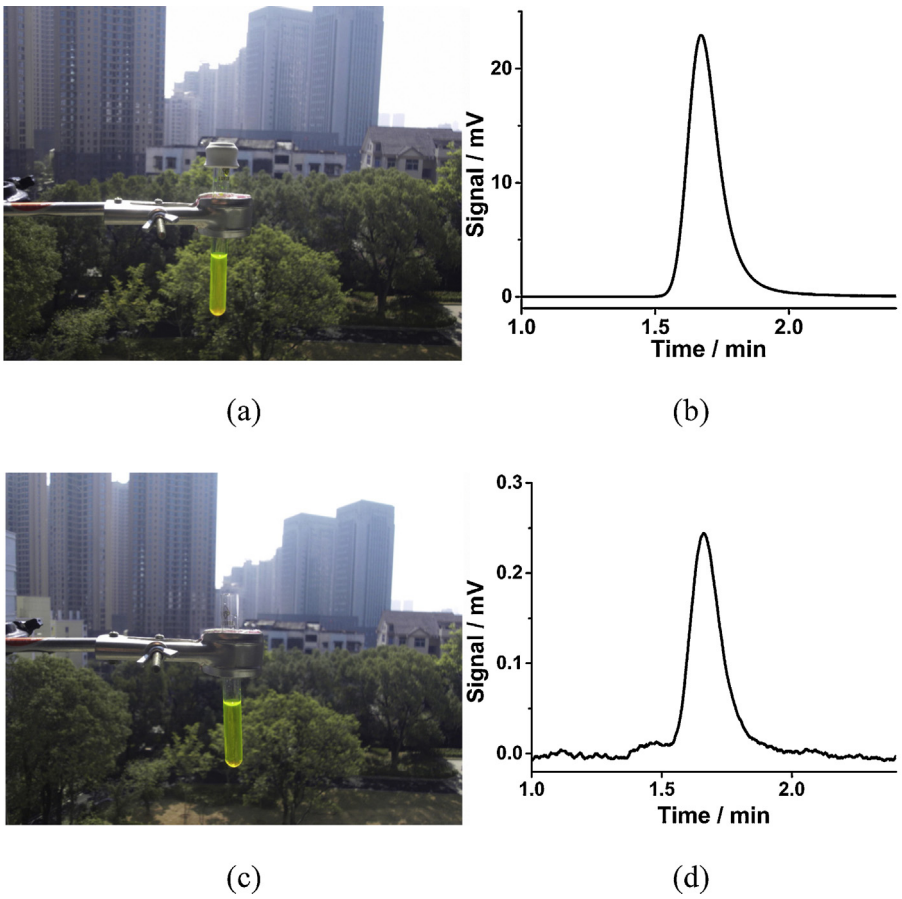


**Fig. 6.** (a) (c) Photo-$H_2$ evolution performed in a test-tube without anoxic treatment under the illumination of sunlight in Fuzhou city from 9:00 to 12:00 on Jan 24, 2016. The signal response of GC from the gas above the liquid in a sealed system (b) and in an open atmosphere (d).

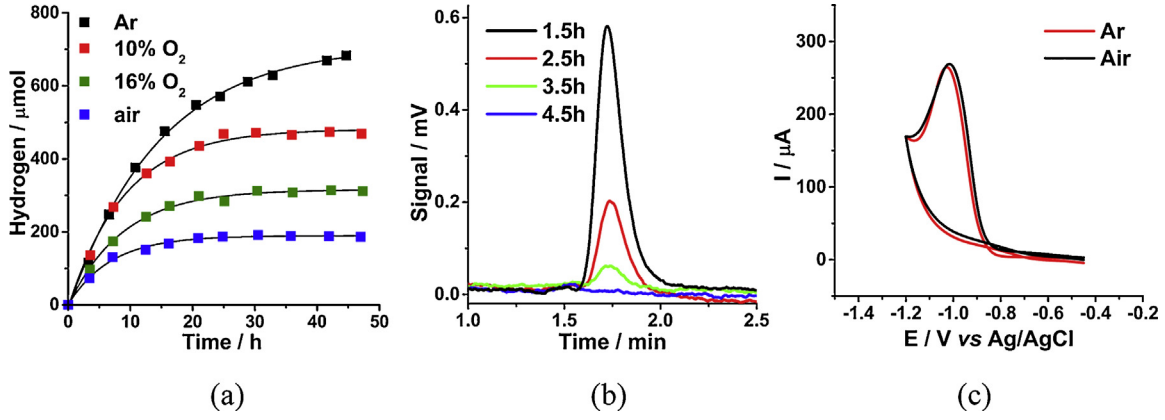


**Fig. 7.** (a) The amount of hydrogen photogenerated under different atmosphere. (b) The signal response of GC from the gas above the liquid in an open system under illumination of LED at one-hour intervals. (c) CVs of **1** in 0.1 M sodium perchlorate solution at a scan rate of 100 mVs$^{-1}$ under argon and air, respectively.

and 28631 M$^{-1}$ for **1** (Figs. S13, S14). At first glance, the catalyst is a more powerful quencher than TEA and an oxidative pathway seems to be dominant in the photocatalytic reaction. However, considering that the amount of TEA is three orders of magnitude higher than **1** in a typical photocatalytic reaction, TEA should have more opportunities to quench the excited fluorescein than the catalyst. Moreover, the zeta potential of **1** was measured to be −20.00 mV in an alkaline NaOH solution. The electrostatic repulsion would enhance the difficulty for the catalyst to access to Fl and thereby impair the quenching ability of the catalyst. As a result, there would be a competition between the oxidative and reductive pathways in the photocatalytic $H_2$ evolution.

To determine the dominant PET process, *in-situ* electron paramagnetic resonance (EPR) experiment was carried out to detect the intermediate radical during photocatalytic process (Fig. 8). When an aqueous solution of Fl and TEA was illuminated by visible light, a signal gradually appeared in the EPR spectrum with a g-factor of 2.0034 and a coupling constant of 3.36 G, which could be assigned to the fluorescein semiquinone ($Fl^{3-\bullet}$) generated by the interaction between TEA and the excited Fl dianion [43]. More specifically, the excited $^*Fl^{2-}$ accepted an electron from TEA and then was reduc-

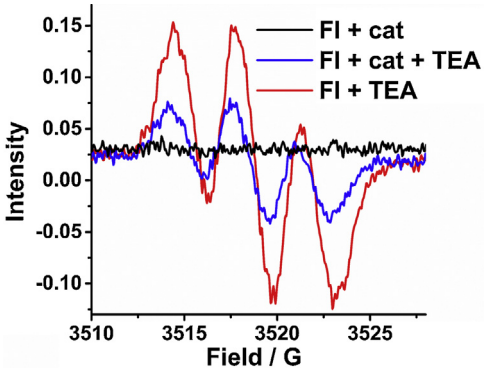


**Fig. 8.** EPR spectra of different solutions at pH = 10 after illumination for 30 min.

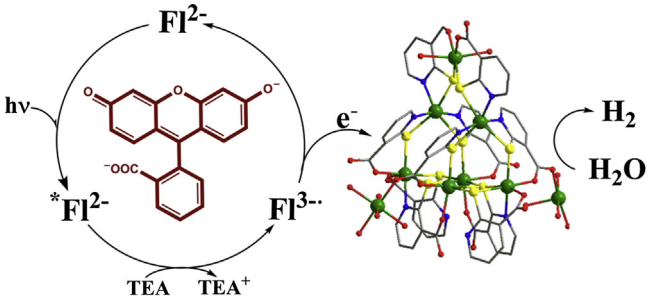


**Scheme 1.** Proposed pathway for the photo-$H_2$ evolution.

tively quenched to form $Fl^{3-}$•. In the presence of **1**, the signal of $Fl^{3-}$• became much weaker than its absence, implying the consumption of $Fl^{3-}$• by transferring electron from $Fl^{3-}$• to the catalyst. Thus, the reductive mechanism might be dominant in the photocatalytic process and the possible pathway for $H_2$ production was illustrated in Scheme 1. Besides, the system was EPR silent before illumination and the signal disappeared soon after the light was turned off, indicating once again that visible light drove the formation of semiquinone and was indispensable in this system (Fig. S15).

## 4. Conclusion

In conclusion, we reported herein a feasible synthesis of a noble-metal-free metal-organic CP to function as an efficient heterogeneous catalyst for the photolysis of water to produce $H_2$ under visible light irradiation. The optimized TON up to 685.4 was obtained, which is higher than most of the photocatalytic $H_2$ evolution systems based on CPs. The catalyst could be recycled for five cycles and the high efficiency could be kept in 240 h. Under air atmosphere, the TON could reach up to 93.5 in the first cycle and little sacrifice in the activity was observed in the second cycle. Solar is able to directly drive this oxic photosystem to produce $H_2$ and all the hydrogen originates from the half-splitting of water, realizing the solar conversion of water to $H_2$. Furthermore, a reductive mechanism is proposed by *in-situ* EPR spectroscopy. This work demonstrates an unprecedented CP as catalyst to produce hydrogen with improved activity and oxygen-tolerance, which has the potential for the application in hydrogen-producing devices without the use of noble-metal complexes.

## Acknowledgments

We thank the National Basic Research Program of China (973 Program, 2012CB821702), the National Natural Science Foundation of China (21233009 and 21571175) and the State Key Laboratory of Structural Chemistry, Fujian Institute of Research on the Structure of Matter, Chinese Academy of Sciences for financial support. We thank Prof Zhaohui Li, Dr. Dengke Wang, Dr. Sibo Wang and Dr. Zhaoyu Wang in Fuzhou university for the help of photochemical test.

## Appendix A. Supplementary data

Supplementary data associated with this article can be found, in the online version, at http://dx.doi.org/10.1016/j.apcatb.2016.05.072

## References

[1] S. Wang, Y. Hou, X. Wang, ACS Appl. Mater. Interfaces 7 (2015) 4327–4335.
[2] S. Wang, X. Wang, Angew. Chem. Int. Ed. 55 (2016) 2308–2320.
[3] Z. Wang, M. Jiang, J. Qin, H. Zhou, Z. Ding, Phys. Chem. Chem. Phys. 17 (2015) 16040–16046.
[4] S. Wang, Z. Ding, X. Wang, Chem. Commun. 51 (2015) 1517–1519.
[5] X. Wu, C. Corcoran, S. Yang, J. Xiao, ChemSusChem 1 (2008) 71–74.
[6] L.E. Kreno, K. Leong, O.K. Farha, M. Allendorf, R.P. Van Duyne, J.T. Hupp, Chem. Rev. 112 (2012) 1105–1125.
[7] M.P. Suh, H.J. Park, T.K. Prasad, D.W. Lim, Chem. Rev. 112 (2012) 782–835.
[8] J.R. Li, J. Sculley, H.C. Zhou, Chem. Rev. 112 (2012) 869–932.
[9] T. Zhang, W. Lin, Chem. Soc. Rev. 43 (2014) 5982–5993.
[10] H.Q. Xu, J. Hu, D. Wang, Z. Li, Q. Zhang, Y. Luo, S.H. Yu, H.L. Jiang, J. Am. Chem. Soc. 137 (2015) 13440–13443.
[11] N. Kornienko, Y. Zhao, C.S. Kley, C. Zhu, D. Kim, S. Lin, C.J. Chang, O.M. Yaghi, P. Yang, J. Am. Chem. Soc. 137 (2015) 14129–14135.
[12] D. Wang, M. Wang, Z. Li, ACS Catal. 5 (2015) 6852–6857.
[13] D. Wang, R. Huang, W. Liu, D. Sun, Z. Li, ACS Catal. 4 (2014) 4254–4260.
[14] H. Wang, B. Li, H. Wu, T.L. Hu, Z. Yao, W. Zhou, S. Xiang, B. Chen, J. Am. Chem. Soc. 137 (2015) 9963–9970.
[15] J. Jiang, O.M. Yaghi, Chem. Rev. 115 (2015) 6966–6997.
[16] C. Gomes Silva, I. Luz, F.X. Llabres i Xamena, A. Corma, H. Garcia, Chem. Eur. J. 16 (2010) 11133–11138.
[17] K. Meyer, M. Ranocchiari, J.A. v. Bokhoven, Energy Environ. Sci. 8 (2015) 1923–1937.
[18] M.A. Nasalevich, R. Becker, E.V.R.-F.S. Castellanos, S.L. Veber, M.V. Fedin, F. Kapteijn, J.N.H. Reek, J.I.v.d. Vlugt, J. Gascon, Energy Environ. Sci. 8 (2015) 364–375.
[19] T. Toyao, M. Saito, Y. Horiuchi, K. Mochizuki, M. Iwata, H. Higashimura, M. Matsuoka, Catal. Sci. Technol. 3 (2013) 2092–2097.
[20] X.L. Hu, C.Y. Sun, C. Qin, X.L. Wang, H.N. Wang, E.L. Zhou, W.E. Li, Z.M. Su, Chem. Commun. 49 (2013) 3564–3566.
[21] A. Fateeva, P.A. Chater, C.P. Ireland, A.A. Tahir, Y.Z. Khimyak, P.V. Wiper, J.R. Darwent, M.J. Rosseinsky, Angew. Chem. Int. Ed. 51 (2012) 7440–7444.
[22] C. Wang, K.E. deKrafft, W. Lin, J. Am. Chem. Soc. 134 (2012) 7211–7214.
[23] Z.M. Zhang, T. Zhang, C. Wang, Z. Lin, S. Long, W. Lin, J. Am. Chem. Soc. 137 (2015) 3197–3200.
[24] S. Pullen, H. Fei, A. Orthaber, S.M. Cohen, S. Ott, J. Am. Chem. Soc. 135 (2013) 16997–17003.
[25] H. Fei, S. Pullen, A. Wagner, S. Ott, S.M. Cohen, Chem. Commun. 51 (2015) 66–69.
[26] K. Sasan, Q. Lin, C. Mao, P. Feng, Chem. Commun. 50 (2014) 10390–10393.
[27] Y. Kataoka, K. Sato, Y. Miyazaki, K. Masuda, H. Tanaka, S. Naito, W. Mori, Energy Environ. Sci. 2 (2009) 397–400.
[28] Y. Feng, C. Chen, Z. Liu, B. Fei, P. Lin, Q. Li, S. Sun, S. Du, J. Mater. Chem. A 3 (2015) 7163–7169.
[29] T. Zhou, Y. Du, A. Borgna, J. Hong, Y. Wang, J. Han, W. Zhang, R. Xu, Energy Environ. Sci. 6 (2013) 3229–3234.
[30] W.X. Zhang, P.Q. Liao, R.B. Lin, Y.S. Wei, M.H. Zeng, X.M. Chen, Coord. Chem. Rev. 293–294 (2015) 263–278.
[31] R. Eisenberg, H.B. Gray, Inorg. Chem. 50 (2011) 9741–9751.
[32] Z. Han, W.R. McNamara, M.S. Eum, P.L. Holland, R. Eisenberg, Angew. Chem. Int. Ed. 51 (2012) 1667–1670.
[33] Z. Han, L. Shen, W.W. Brennessel, P.L. Holland, R. Eisenberg, J. Am. Chem. Soc. 135 (2013) 14659–14669.
[34] H.N. Kagalwala, E. Gottlieb, G. Li, T. Li, R. Jin, S. Bernhard, Inorg. Chem. 52 (2013) 9094–9101.
[35] Y.J. Yuan, Z.T. Yu, X.J. Liu, J.G. Cai, Z.J. Guan, Z.G. Zou, Sci. Rep. 4 (2014) 4045.
[36] S. Wang, W. Yao, J. Lin, Z. Ding, X. Wang, Angew. Chem. Int. Ed. 53 (2014) 1034–1038.
[37] W. Zhang, Y. Wang, Z. Wang, Z. Zhong, R. Xu, Chem. Commun. 46 (2010) 7631–7633.
[38] S. Chatterjee, K. Sengupta, S. Dey, A. Dey, Inorg. Chem. 52 (2013) 14168–14177.
[39] A. Das, Z. Han, W.W. Brennessel, P.L. Holland, R. Eisenberg, ACS Catal. 5 (2015) 1397–1406.
[40] D.W. Wakerley, E. Reisner, Energy Environ. Sci. 8 (2015) 2283–2295.
[41] P. Cui, H.S. Hu, B. Zhao, J.T. Miller, P. Cheng, J. Li, Nat. Commun. 6 (2015) 6331.
[42] B.R.S. Avidsona, K. Trethewey, Chem. Commun. 31 (1975) 674–675.
[43] M. Okuda, Y. Momose, S. Niizuma, M.B. Koizumi, Chem. Soc. Jpn. 40 (1967) 1332–1336.